Available online at www.sciencedirect.com
ScienceDirect
Dynamics of Atmospheres and Oceans
42 (2006) 3–29
dynamics of atmospheres and oceans
www.elsevier.com/locate/dynatmoce

The mesoscale convection life cycle: Building block or prototype for large-scale tropical waves?

Brian Mapes [a,*], Stefan Tulich [b], Jialin Lin [b], Paquita Zuidema [a]

[a] *Rosenstiel School of Marine and Atmospheric Sciences, University of Miami, Miami, FL, United States*
[b] *NOAA ESRL and CIRES, University of Colorado, Boulder, CO, United States*

Available online 6 September 2006

Abstract

A cumulonimbus cloud may ascend and spawn its anvil cloud, precipitation, and downdrafts within an hour or so. This paper inquires why a similar progression of events (life cycle) is observed for tropical weather fluctuations with time scales of hours, days, and even weeks. Regressions using point data illustrate the characteristic unit of rain production: the mesoscale convective system (MCS), covering tens of kilometers and lasting several hours, with embedded convective rain cells. Meanwhile, averages over larger spatial areas indicate a self-similar progression from shallow to deep convection to stratiform anvils on many time scales.

Synthetic data exercises indicate that simple superpositions of fixed-structure MCS life cycles (the Building Block hypothesis) cannot explain why longer period life cycles are similar. Rather, it appears that an MCS may be a small analogue or prototype of larger scale waves. Multiscale structure is hypothesized to occur via a Stretched Building Block conceptual model, in which the widths (durations) of *zones* of shallow, deep, and stratiform anvil clouds in MCSs are modulated by larger scale waves.

Temperature (T) and humidity (q) data are examined and fed into an entraining plume model, in an attempt to elucidate their relative roles in these large-scale convection zone variations. T profile variations, with wavelengths shorter than troposphere depth, appear important for high-frequency (∼2–5-day period) convectively coupled waves, as density directly links convection (via buoyancy) and large-scale wave dynamics (via restoring force). Still, the associated q anomalies are several times greater than adiabatic, suggesting a strong amplification by shallow convective feedbacks. For lower frequency (intraseasonal) variability, q anomalies are considerably larger compared to T, and may be dominant.

Keywords: Atmospheric convection; Tropical meteorology; Mesoscale convective systems

* Correspondence to: RSMAS/MPO, 4600 Rickenbacker Cswy, Miami, FL 33149-1098, United States. Tel.: +1 305 421 4275; fax: +1 305 421 4696.
E-mail address: mapes@miami.edu (B. Mapes).

0377-0265/$ – see front matter © 2006 Elsevier B.V. All rights reserved.
doi:10.1016/j.dynatmoce.2006.03.003

1. Background and motivation

Tropical convective cloud activity fluctuates on a very broad range of space and time scales. Large-scale cloudy disturbances, including waves that propagate according to dispersion relations from simple linear theory (Takayabu, 1994; Wheeler and Kiladis, 1999), stand as scientific challenges and are important to weather and climate applications. Such waves are poorly and inconsistently simulated by global models with parameterized convection (Lin et al., 2006). Reasons for this shortcoming of contemporary tropical meteorology appear to include a lack of fundamental understanding of mechanisms of wave-convection interaction, not just difficulties of numerical implementation.

Observations of convection and convectively coupled waves are abundant, but there are challenges in translating these into knowledge suitable for model building. Absolute accuracy of thermodynamic measurements is one perpetual problem (Ciesielski et al., 2003; Guichard et al., 2000), while spotty undersampling within a broad spectrum of scales introduces further random errors (Mapes et al., 2004). Statistical analysis can overcome these challenges, and also helps to highlight repeatable, key features among all the details of individual weather events. However, this activity is hindered by a lack of suitable diagnostic frameworks in which observations meaningfully answer questions about cause and effect. Waves of a given period and scale are defined as filtered anomalies fluctuating within a convecting background state, among a sea of other anomalies on other scales. Such a description is not easy to square with observations of coherent cloud entites in the sky at particular places and times.

These thorny issues are often lumped in the term 'scale interactions.' However, this is a very broad category, encompassing all manner of mechanisms – linear and nonlinear – throughout and beyond the atmosphere (Meehl et al., 2001). For definiteness and simplicity, we will preferentially resort, at least initially, to hypotheses and explanations that might better be called *linear scale superpositions*. Deep convection, as a positive-definite heat source, simultaneously excites waves in the atmosphere with a very broad spectrum of wavelengths and frequencies. Large-scale patterns of convection excite large-scale components that may reinforce coherently, while random convective events (or random failures of convection) introduce smaller scale noise. In this view, the only actual *interaction* of scales is via modulations of broadband convective sources. Linear regression – the main analysis tool used here – implicitly reflects such a linear superposition viewpoint. Here the "characteristic" scale of convection is simply a decorrelation length, as in Ricciardulli and Sardeshmukh (2002). However, it must be remembered that such characteristic scales are resolution dependent, since filtering small-scale noise out of a data series by coarsening its resolution increases the decorrelation length.

In addition to being a heat source, convection also exerts tendencies in the momentum equation, through vertical fluxes of horizontal momentum. Momentum flux, like heating, is a broadband influence, with rectified or "upscale" effects. The flux by tilted, organized penetrative convective drafts can be up-gradient, acting quite unlike simple friction, as emphasized, for example, in some recent studies of the Madden–Julian Oscillation (Biello and Majda, 2005, 2006; Houze et al., 2000; Moncrieff, 2004). However, momentum flux effects are not necessarily cumulative like heating: vertical circulations on different nested scales may be tilted oppositely, and cancel rather than reinforce. Cloud models show that the effect of small-scale convective motions appear to be mainly frictional, even in two dimensions (Mapes and Wu, 2001), so the true importance of exotic fluxes by tilted structures in mesoscale (filtered) versions of the total flow remains unclear. For reasons mainly of uncertainty, then, we leave questions of momentum flux in the background in this paper, although these are prominent among the implications of the tilted structures diagnosed here.

The life cycle of individual cumulonimbus clouds is considered background knowledge for this article; see, e.g. Houze (1993). Elemental (minimum) time scales for this life cycle spring from cumulus dynamics (the penetrative buoyant ascent of a finite-sized air parcel through an environment); and from cloud microphysics, especially the development and fall of precipitation. A cumulus dynamics time scale is the depth of the convecting layer divided by vertical velocity (w). Estimating w is not trivial, but observations indicate a few m/s, yielding typical cloud ascent times of many minutes to an hour or more. Microphysical time scales include the time for cloud particles to consolidate into precipitation, and the sedimentation time of precipitation. Again, these time scales range from tens of minutes to hours, with the fallout of small ice particles being especially slow (leading to long-lived anvil clouds).

Because of these finite time delays, and economies of scale arising from entrainment which favor large and grouped clouds, the smallest unit of tropical precipitating convection is not the infinitesimal updraft predicted by linear theory, with its shortwave catastrophe (Lilly, 1960), nor even the isolated unicellular shower. Rather, the ultimate building block of deep convective weather is a multicellular cumulonimbus event (Figs. 8.5 and 8.7 of Houze, 1993). Multicellular cumulonimbus often occur in groups called mesoscale precipitation features (MPFs), with contiguous or merged rain areas, cold-air outflow pools at the surface, and anvil clouds in the upper troposphere (Leary and Houze, 1979). One or more MPFs may be given the generic label of a mesoscale convective system (MCS), a term we will preferentially use here for its greater familiarity. Houze (2004) offers a recent review of MCSs. In the active phases of larger scale waves, MCSs may in turn occur in groups, often with ambiguous boundaries, in a broad continuous size spectrum exhibiting no preferred 'mesoscale' (Mapes and Houze, 1993; Wilcox and Ramanathan, 2001). The subject of this manuscript is why these larger groupings have life cycles that appear similar to the stages of a cumulonimbus cloud.

2. Conceptual models from prior studies

An early conceptual model of MCS structure is shown in Fig. 1a, from the Zipser (1969) study of an arc-shaped squall in the Line Islands. Convection growing at the leading edge is seen to decay into "old towers," merging into a precipitating stratiform anvil. The stylized depiction in Fig. 1a almost suggests that MCS structure is merely an aliasing of the life cycle of an individual convective cloud, spread out in space as if along an assembly line, with new clouds periodically initiated at a propagating source (the gust front).

A more detailed MCS schematic is in Fig. 1b, from Zipser et al. (1981). The multicellular nature of the phenomenon is depicted more clearly here: for example, the leading edge is shown as a *zone* of middle-topped cumulus clouds, not merely the next deep updraft seen halfway through its ascent process.

A similar depiction of zones of shallow, deep, and stratiform clouds is echoed in Fig. 1c, from the Takayabu et al. (1996) study of 2-day waves over the western Pacific. Here the horizontal axis is time rather than space, since it is easier to collect time series at a point than measure across thousands of kilometers of ocean instantaneously, but satellite data indicate that spatial structure mimics this temporal structure. The 2-day wave illustrates very well the ambiguous boundary between MCSs and large-scale waves: its wavelength is not vastly greater than the size of individual cloud shields seen in satellite imagery, yet its flow fields approximately satisfy dispersion relations from linear equatorial wave theory, specifically the westward inertio-gravity wave—see also Haertel and Johnson (1998) and Haertel and Kiladis (2004).

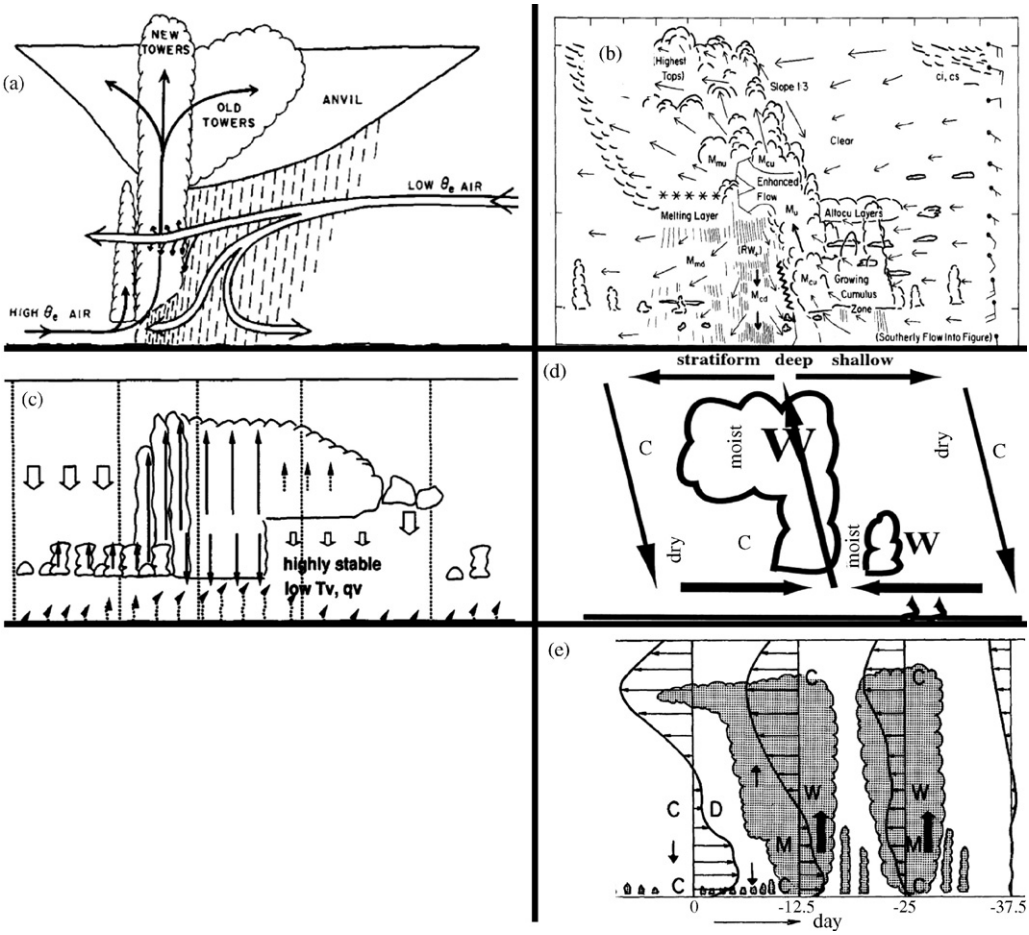

Fig. 1. Conceptual models of: (a and b) mesoscale convective systems (Zipser, 1969; Zipser et al., 1981); (c) a 2-day wave (Takayabu et al., 1996); (d) a convectively coupled Kelvin wave (Straub and Kiladis, 2003); (e) the Madden–Julian Oscillation (Lin and Johnson, 1996).

For larger, slower synoptic tropical waves (few day periods), the picture is again similar, as illustrated by Fig. 1d, from the Kelvin wave study of Straub and Kiladis (2003). Rotational (easterly) waves are similarly tilted, with the rising of upward motion across the wave resembling the rising with time of MCS upward motions (Houze, 1982). Finally, still-larger scales of organization are illustrated in Fig. 1e, from the Lin and Johnson (1996) study of an intraseasonal (Madden–Julian Oscillation, MJO) convective event and low-level westerly wind burst over the western Pacific. At the front of the whole system (before day −25), shallow clouds give rise to deeper clouds. This upward development cycle is repeated again around day −15, but with more extensive upper-level anvil cloud after the second cycle, producing an overall intraseasonal shallow-to-anvil progression across about 40 days. See also Fig. 14 of Morita et al. (2006).

These schematics attest (as is confirmed below) that the dataset underlying Fig. 1c and e depicts convective developments resembling a thunderstorm life cycle on at least three long time scales: 2, ∼10, and ∼40 days. Meanwhile, finer resolution data from throughout the tropics depict the

MCS life cycle with its characteristic time scale of hours. Is the resemblance of all these cloud structures a meaningless coincidence, an inevitable consequence of the basic convective process, or something in between?

After an outline of data and methods, Section 4 illustrates the basic tilted structure of the MCS life cycle as sampled in tropical field data. Section 5 examines observations spanning multiple scales, to illustrate the similarity across scale. Section 6 constructs realizations of Building Block null hypotheses, and compares them to large-scale observations. Section 7 examines how the MCS life cycle is embedded in larger scale wave dynamics in a large-domain cloud model, where sampling and data accuracy are perfect. Section 8 compares observations to the model, and discusses the relative roles of temperature versus moisture.

3. Data and methods

Many results in this paper are contoured time–height sections of the slopes of linear regressions between a reference time series of surface rainfall, and time series of other data from other altitudes and time lags. The other data (*predictand*) can be any field, and the units of the regression slope are the units of the predictand per unit of rainrate. Values at negative lag indicate data excursions prior to rainfall, while positive lags indicate excursions following rainfall.

These regression slope diagrams, which we sometimes call *statistical composites* or *characteristic structures*, have many advantages. The regression averages out random data errors and variability unrelated to rainfall, reducing complex and often noisy time–height datasets to relatively simple, clear characteristic structures. Missing data present no problem, other than difficulty of interpretation in the case of weather-dependent data dropouts. Datum-specific error estimates can be incorporated easily, as is done for the radar results; see Mapes and Lin (2005) for details. (For most datasets here, the errors are assumed uniform so that all values are weighted equally in the regression line fitting process.) Such a regression approach has been widely used for large-scale data analysis; e.g. Kiladis and Weickmann (1992) and many others.

One concern we initially had about linear regression is that it could give distorted results when using a skewed variable like rainrate, which is nonnegative and has many zero values. To explore this concern, we compared other techniques, such as composite averaging around keydates defined from positive rainfall excursions, using both real and synthetic data. We also experimented with data-quality hazards, for example, splicing sequences of zeroes into datasets before input to the regression, trimming and padding the ends of the data, and truncating negative rainrates (which exist in budget datasets because of estimation errors). Results of these experiments indicate that the regression-coefficient structures shown in this paper are robust and not unduly sensitive to arbitrary analysis choices. We are mostly analyzing strong and unsurprising signals. The coherence of features in the lag-height domain, and their agreement with existing knowledge, are in this case more relevant indicators of significance than formal statistical tests, which are not presented.

Temporal filtering is lightly and sparingly employed, but is necessary in some cases where very low frequency signals obscure faster changes around rain events (a exacerbated by the logarithmic contour interval chosen here for its clarity in other respects). In such cases, the rainrate time series is filtered using a Lanczos filter with cutoff frequencies as indicated in the text and captions (usually periods longer than several times the plotted domain are excluded). There is no need to filter predictands, as the absence of a frequency in the predictor time series will eliminate correlations at that frequency, even if it is present in the predictand time series.

Our sources of time–height data and rainrate base time series include both observations and models. The main source of observations is tropical field programs from the past decade or two,

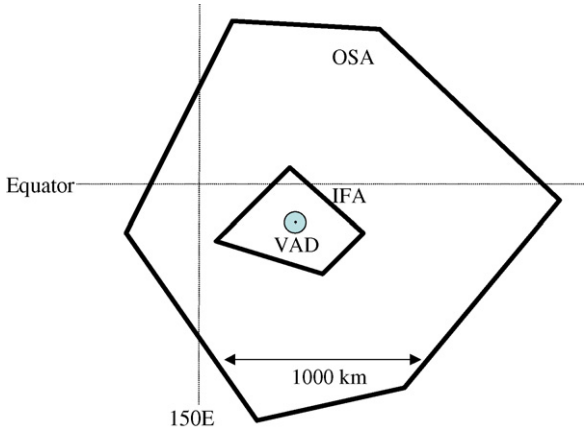

Fig. 2. Location and scales of some observational data used here.

especially radar and sounding budget data from TOGA COARE (Webster and Lukas, 1992), as well as data from the more recent EPIC (Raymond et al., 2004) and JASMINE (Webster et al., 2002) experiments, where unique high-resolution datasets from a shipborne vertically pointing K-band (8.66 mm wavelength) cloud radar were available (Zuidema et al., 2006). Observations at this wavelength are unusual (and unlikely to be repeated) in having the sensitivity to see cloud, not just precipitation, but with the relatively mild attenuation of near-centimeter wavelength allowing the higher altitude parts of deep cloud systems to be seen. Doppler weather (precipitation) radar data from many areas have also been utilized here; Mapes and Lin (2005) offer details and further references about these datasets. The Doppler data were processed using Velocity-Azimuth Display (VAD) methods, to yield time–height sections of horizontal wind divergence averaged over circular areas of ∼48 km radius centered on the radar at hourly time resolution.

Wind divergence was also estimated from arrays of balloon soundings at larger scales, illustrated in Fig. 2 as the COARE Intensive Flux Array (IFA) and Outer Sounding Array (OSA). These divergence estimates were converted to rainrate estimates using gridded methods as described by Johnson and Ciesielski (2000) and other publications by the Johnson research group. The time resolution of this COARE sounding budget dataset is 6 hourly spanning 120 days (480 points in time).

Cloud-resolving model output are from Tulich et al. (in press), a study of simulated radiative convective equilibrium on a large two-dimensional domain. Grid spacing was 2 km, while data were sampled at 30 min intervals. Large-scale waves modulating envelopes of convection emerged spontaneously in these experiments, similar to the results of Grabowski and Moncrieff (2001).

4. Vertical tilt and the MCS life cycle

Horizontal wind divergence is an informative variable to examine, since it is the main manifestation of atmospheric heating in tropical convection that is observable above the noise level (Mapes et al., 2004). Wind divergence and its relationship to surface rainrate are illustrated in Fig. 3. Lag-height regression composites using the entire time span of the available COARE data are shown in left, while selected data samples are presented in the right-hand panels. Similarities and

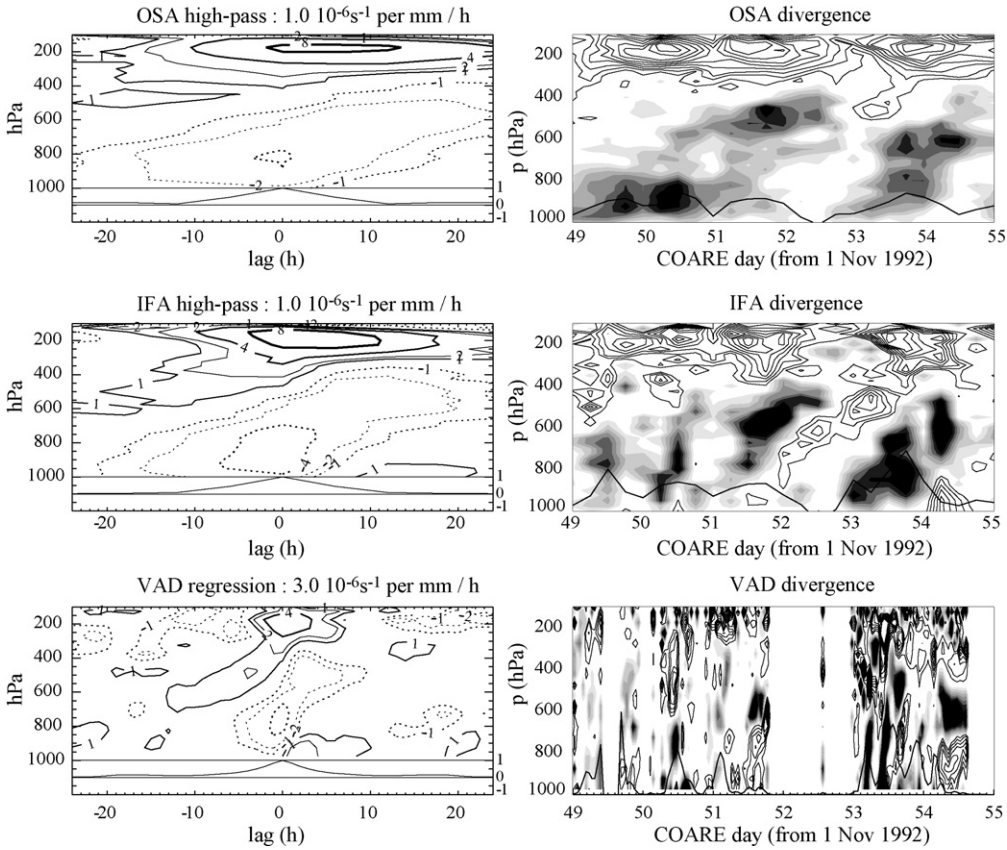

Fig. 3. Divergence-rain associations at three spatial scales. Left column: lag-height regressions vs. surface rainrate. Rain autocorrelation is the curve at bottom of each plot, on scale [−1, 1] indicated at right. Lanczos filtering was used to first remove periods longer than 24 days from IFA and OSA rainfall series. Right column: raw data samples from days 49 to 55 of COARE (19–25 December 1992). Filled contours are negative values, open contours are positive values at twice the contour interval; contours rescaled in each panel for clarity. Heavy curves at bottom of each panel are rainrate time series.

differences are seen among the COARE OSA, IFA, and VAD spatial areas indicated in Fig. 3. The most obvious difference is that larger spatial scales are dominated by longer time scales. Light high-pass filtering was used on the IFA and OSA rainrate time series for panels a and b, to remove very long periods (more than 5 times the width of the lag window shown).

All panels show that rain events are accompanied by lower-troposphere convergence and upper-level divergence, indicative of upward motion. But a distinctive tilt is also evident: wind convergence (dotted contours in left panels, shading at right) tilts upward to the right, as low-level convergence in advance of peak rainrate gives way to middle-level convergence afterward, in precipitating stratiform anvil clouds (Houze, 1997). The convective and mesoscale downdrafts during and after rain lead to positive divergence anomalies near the surface, at least at VAD and IFA scales.

Another notable tilt in Fig. 3 is the rising with time before precipitation of the altitude of positive divergence. This presumably corresponds to the rising outflow level of deepening con-

vection. Secondary maxima near the 500 h Pa level in advance of peak rainfall suggest a preferred population of cumulus congestus clouds, although the signal is noisy. Such a distinct congestus mode of convection in COARE was also highlighted by Johnson et al. (1999). They noted that "Congestus clouds are most prevalent when there is MCS organization and cumulonimbus activity," but because of the long time series they presented, the slight lag indicating the coherent role of congestus clouds in the MCS life cycle is hard to see in their results.

To gain a more robust depiction of the characteristic evolution of divergence in MCSs, Fig. 4a shows a lag-height section obtained by averaging the lag-height regression results from seven monthlong oceanic radar deployments (individual results may be seen in Mapes and Lin, 2005). Again a distinct secondary peak of divergence at midlevels is seen 8 h before maximum rainfall, and is present in many of the individual cases as well. The structure in Fig. 4a can be vertically integrated to yield pressure vertical velocity ω, after adjusting the divergence almost imperceptibly and uniformly in height to enforce zero boundary conditions at the surface and 100 h Pa (Fig. 4b). Note that Fig. 4b uses a positive sign to denote upward motion (mass flux) for visual clarity. Downward motion is seen to extend as high as the 500 h Pa level in the hours after peak rainfall.

The structure in Fig. 4 is in the time domain, but its relationship to spatial flow structures can be illustrated by interchanging time and space (as has been done in juxtaposing the schematics of Fig. 1). A pattern of horizontal divergent wind $u'(x, p)$ can be derived by integrating divergence horizontally at each p level. The undetermined constant of integration at each level is handled initially by setting the horizontal average $[u'] = 0$ over the plotted domain. The resulting vector wind field (u', ω) in the $x - p$ plane is shown with arrows in the center panel of Fig. 5. The horizontal distance scale and corresponding absolute value of u are arbitrary, as the slopes of the arrows used to display the 2D nondivergent vector field are ultimately adjusted for viewing convenience. In the other panels of Fig. 5, a height-independent mean wind U_0 and linear shear $U_s(p)$ are added to the center panel's flow field. These background winds are scaled by ± 1 and ± 3 standard deviations, respectively, of u'. The combinations yield nine panels total.

The diverse flow fields in Fig. 5 include all combinations of 'jump' and 'overturning' updrafts and downdrafts discussed in Moncrieff (1992) and elsewhere. All these flows are equally consistent

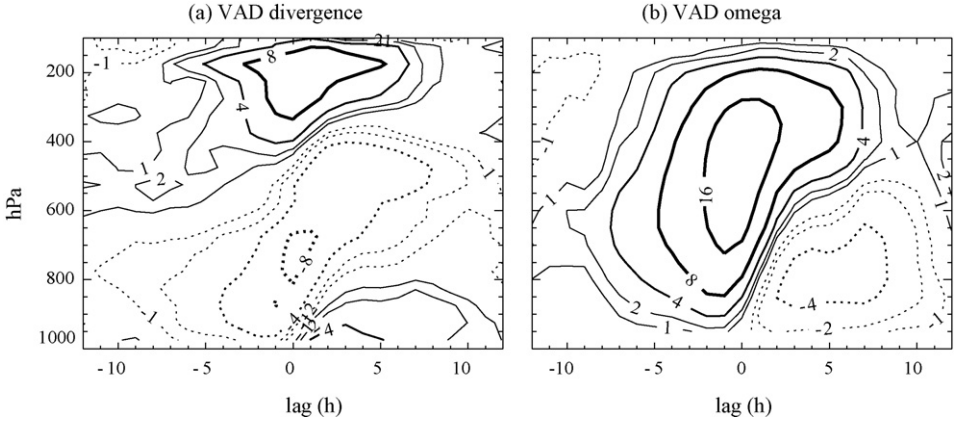

Fig. 4. Regression composite of the MCS life cycle in divergence and vertical motion. Plotted are averages of regression sections from seven tropical radar deployments (see Mapes and Lin, 2005 for details). (a) VAD divergence regressed against rainrate for a circular area of 96 km diameter, contour unit 10^{-6} s^{-1} per mm/h. (b) The corresponding mass flux (pressure units, but with positive sign indicating upward motion), contour unit 10 h Pa/day per mm/h.

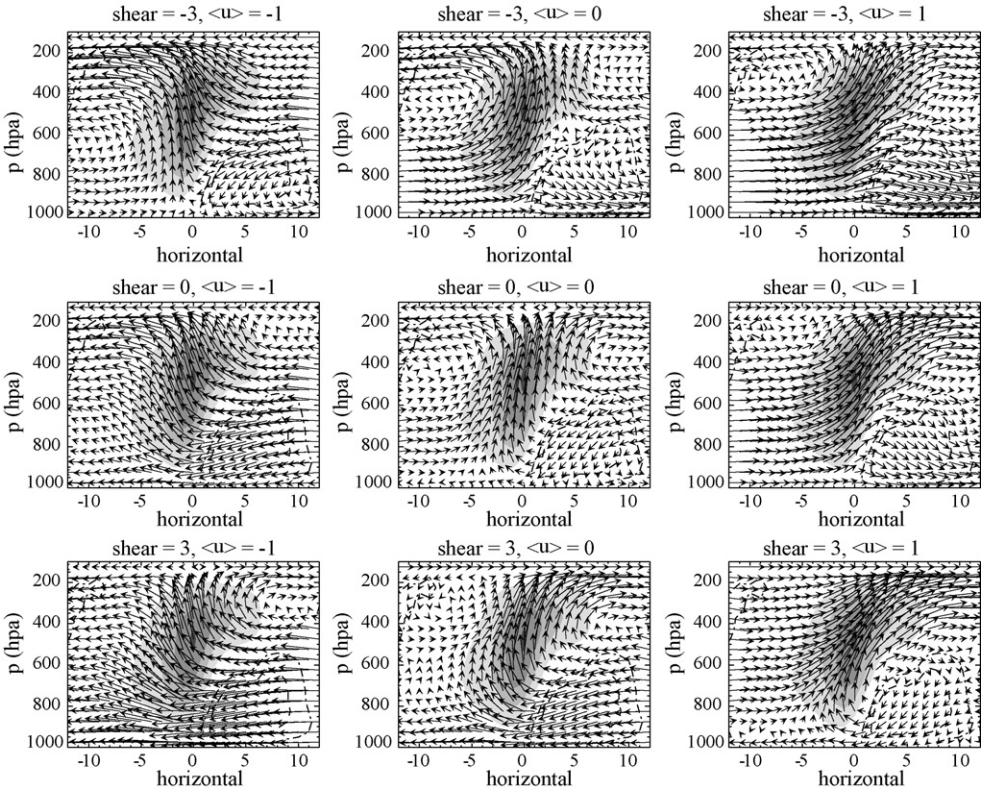

Fig. 5. Vertical motion field from Fig. 4b (shading and dashed contours), overlain by arrows depicting a 2D vector flow field which satisfies mass continuity with it, if the horizontal plot axis is reinterpreted as a spatial dimension. The central plot has zero average horizontal wind at each level. Other panels show this same flow field plus linear (in pressure) shears, indexed by their vertical average U0 and shear strength, each in units of the standard deviation of horizontal wind in the central panel.

with the statistical composite divergence observations, differing only in the horizontal-mean wind U(p). This figure's construction exercise shows that observations of varying streamline patterns in MCSs do not conflict with the idea of quasi-universal profiles of vertical mass flux or heating. Momentum flux is a major reason that flow pattern differences like Fig. 5 are often scrutinized. Indeed, the momentum flux profiles $[u\omega]$ implied by the panels of Fig. 5 do vary, but in a very simple way. The eddy flux $[u'\omega']$ by deviations from the horizontal mean at each pressure is identical in all panels. The differences in total flux $[u\omega]$ therefore spring solely from differences in $[\omega]$ $[U_0 + U_s(p)]$: that is, the flux of the background wind's momentum by the mean upward motion averaged across the whole MCS. In other words, the momentum flux differences in Fig. 5 *do not depend on mesoscale structure* in the flow field.

The decorrelation time scale in Fig. 4 is about 6 h, with the picture losing coherence entirely by ± 12 h. Is this decay time scale fundamental, or is it limited by data resolution? Multiple time scales appear to be present: the convergence layer tilts upward steeply near the time of peak rainrate, but much more slowly with time before and after. While the $\sim$100 km circular areas and 1 h time averages used for Fig. 4 are approaching the typical scales of contiguous rain areas, many smaller scales are still truncated.

To address this concern, point data with 5-min time resolution are analyzed in Fig. 6. Specifically, data from a rain gauge are used as a base time series, and regressed against cloud structure from a vertically pointing cloud (8.33 mm wavelength) radar. For more details on the EPIC cloud radar data see Zuidema et al. (2006). Because this wavelength is attenuated in rain, we use only the coverage by detectable echo, discarding the absolute value of reflectivity which may be in error. The result is a statistical composite of fractional coverage by echo (cloud and/or rain, gray shading). The narrow cone of negative values at zero lag in panel (a) is a consequence of attenuation, and should be discounted, but it illustrates (along with the gauge-based rain-event composite curve aligned below) that there is a distinct convective time scale of <1 h in rainrate; reminiscent of Fig. 15 of McAnelly and Cotton (1992). May and Rajopadhyaya (1999) also found that Eulerian decorrelation times for convective drafts are just a few minutes. Still, Fig. 6 emphasizes that this convective timescale tends to be firmly embedded within the longer mesoscale envelope (several hours). In EPIC (Fig. 6a), the top of the regression-indicated cloud mass (shading) slopes upward over about 6 h, supporting the inference that sloping divergences seen in Figs. 3 and 4 correspond to increasing cloud top heights.

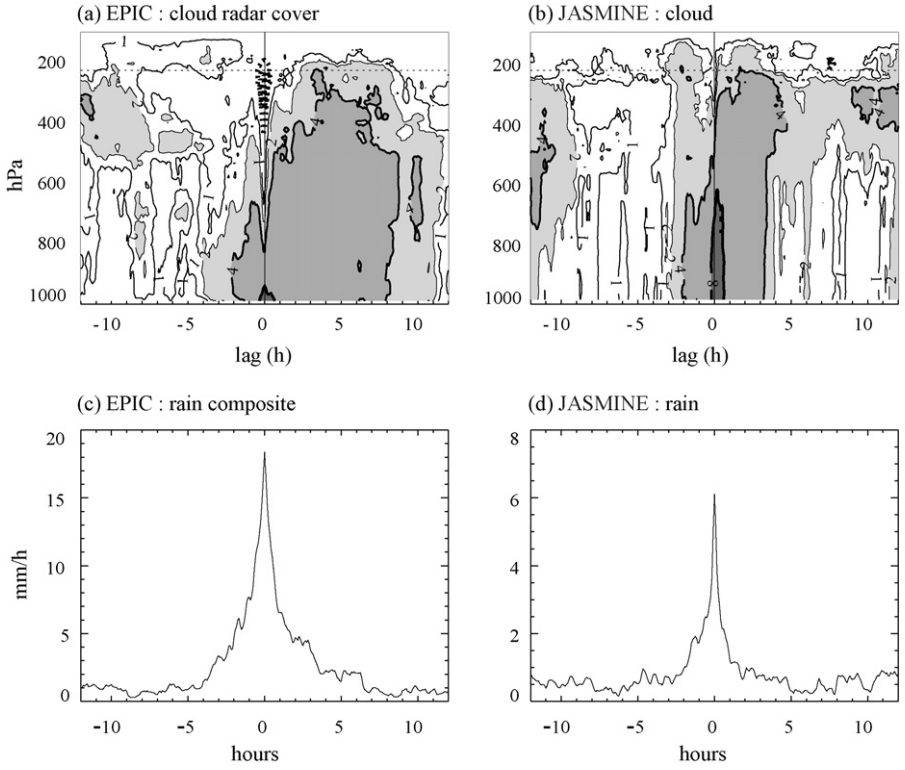

Fig. 6. Cloud and rain composites in point data from the EPIC (a and c) and JASMINE (b and d) field programs. (a and b) Lag-height regressions of echo coverage seen by a vertically pointing cloud radar. Contour unit is 1% per mm/h for JASMINE and 0.25% per mm/h for EPIC (spikes cause large variance in these 5 min rainrate series). (c and d) Composites of gauge rainfall around time intervals when rainrate exceeded 1 standard deviation (5.2 mm/h for EPIC and 2.1 mm/h for JASMINE).

Comparable plots from the JASMINE rain gauge and cloud radar data are shown in the right panels. Here the rainrates (both peak and background) were about half as great, and the central feature of the cloud cover composite is almost free of any rain attenuation feature near zero lag. The time scale of JASMINE events was shorter. Very tall convective clouds preceded surface rain in the dataset's most prominent event, and thereby in this composite figure. The two experiments show many interesting differences and features. There is an apparent node in the cloud field at 225 h Pa (suggested by the dotted line). A clearing of otherwise persistent background middle-upper-level cloudiness at negative lags is seen in both panels a and b, perhaps hinting at subsidence ahead of convective events. The main point of Fig. 6 for the present discussion is simply the gross similarity of time scale (hours, far beyond the data's resolution limits).

In summary, tropical deep convection is seen to have a characteristic vertical development (tilt in the lag-height plane), with a fast convective cell time scale of <1 h embedded in mesoscale storms lasting several hours. Convection grows upward, followed by the development of precipitating stratiform anvils and downdrafts in the lower troposphere. However, the MCS time scale is merely the short end of a broad spectrum of time scales on which a similar tilt is observed, extending out to a day or more. In general, observations at larger spatial scales tend to be relatively enriched in lower frequencies. The next section expands the time axis farther beyond the life span of individual MCSs.

5. Vertical tilt on longer time scales

A convenient vertically resolved proxy for clouds is specific humidity (q), as measured by balloon-borne sondes. Since local fluctuations can be large, results are clearest when averaged over many independent balloon samples (i.e. over a large spatial area like the COARE OSA).

Multiscale lag-height regressions of OSA q are shown in Fig. 7. The familiar tilt, upward to the right, is seen in positive moisture anomalies associated with rainfall. Broadly speaking, the shape is similar to that of the vertical velocity contours in Fig. 4c, and again apparently indicates the upward development of clouds before peak rain, followed by upper-level anvil clouds after rain, overlying dry unsaturated downdrafts in the lower levels.

The top panels separately illustrate three prominent periods of variation (<6, ~12, and ~40 days). Bandpass filtering is accomplished by successively regridding the data from 6 hourly (left) to daily (middle) to 4-day means (right), along with light Lanczos high-pass filtering that removes periods >6 times the width of each lag window. The relationship among these three scales can be seen in the bottom panel, which shows unfiltered data at full (6 hourly) resolution, regressed across ±23 days of lag. Sharply tilted contours near the origin correspond to fast changes associated with large MCSs and 2-day waves. A more gently tilted structure stretching from about -6 to 6 days indicates a prominent ~12-day periodicity (as in Fig. 1d, derived subjectively from these same data). At a still longer time scale, the earliest of three ~12-day wave crests (centered at lag -12 days) has a lower centroid than the latest crest (at day +12), yielding an upward tilt across ~24 days, the active phase (half-period) of the Madden–Julian Oscillation. Each of these three main periodicities can be detected in very close scrutiny of the rainrate autocorrelation curve at bottom.

The presence of low, middle and high frequencies in COARE convective variability can also be seen in raw OSA divergence data (Fig. 8a) from the events of 5 December 1992–5 January 1993. Upward-rightward tilting convergence features (shading) rise up out of a general prevailing low-level convergence, in association with diagnosed rainfall events (curve at bottom of panels).

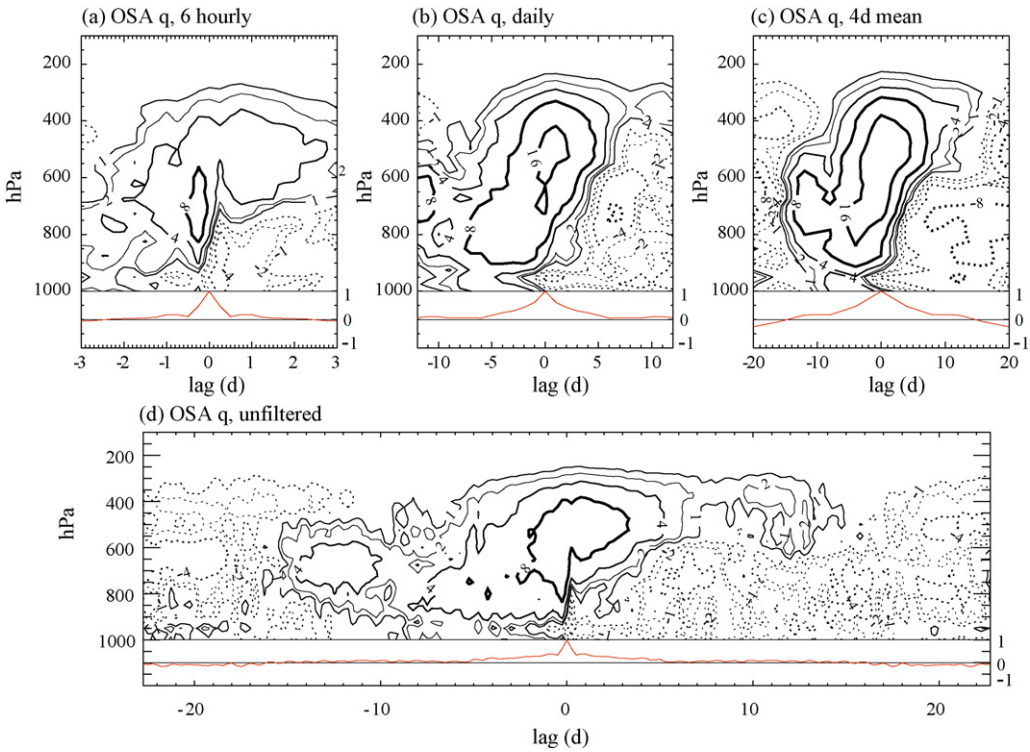

Fig. 7. Lag-height regressions of OSA specific humidity vs. moisture budget-derived rainrate. The data are progressively regridded to coarser time intervals ((a) 6 h, (b) 1 day, and (c) 4 days), and a light high-pass filter is used for each panel (cutoff period six times the lag window width). (d) The original unfiltered 6 h data are used, with a very wide lag window. Contour unit is 0.1 g/kg per mm/h.

Divergence features (open contours) also sometimes rise up with time, merging into a general prevailing upper-level divergence. In the lower three panels, a mutually exclusive and complete set of three temporally filtered components highlights the main time scales prominent in the data.

A notable feature on days 37–38 and 58–65 in Fig. 8 is a quadrupole ($-\ +\ -\ +$) structure in the divergence profile, implying two upward motion peaks: in the lower and upper troposphere. This feature is not seen in the composite MCS life cycle (Fig. 4a), and may be peculiar to the late stages of the Madden–Julian Oscillation or to the COARE weather events in particular. However, we have seen some clear examples of this type of profile after the end of stratiform rain in radar VAD data, as can be glimpsed in Mapes and Lin (2005), so this structure may have its mesoscale counterpart.

To illustrate the cloud fields corresponding to these divergence data, Fig. 9 shows dawn visible images on the dates indicated by black bars in Fig. 8a. The convective-to-stratiform evolution implied by the bars on days 51–52 qualitatively agrees with the sense of the images, with bright mesoscale anvil clouds characterizing Fig. 9b. Thinner cirrus clouds overlying shallow convection in Fig. 9c and d may be seen, apparently corresponding to the two peaks in the profile of upward motion implied by Fig. 8a.

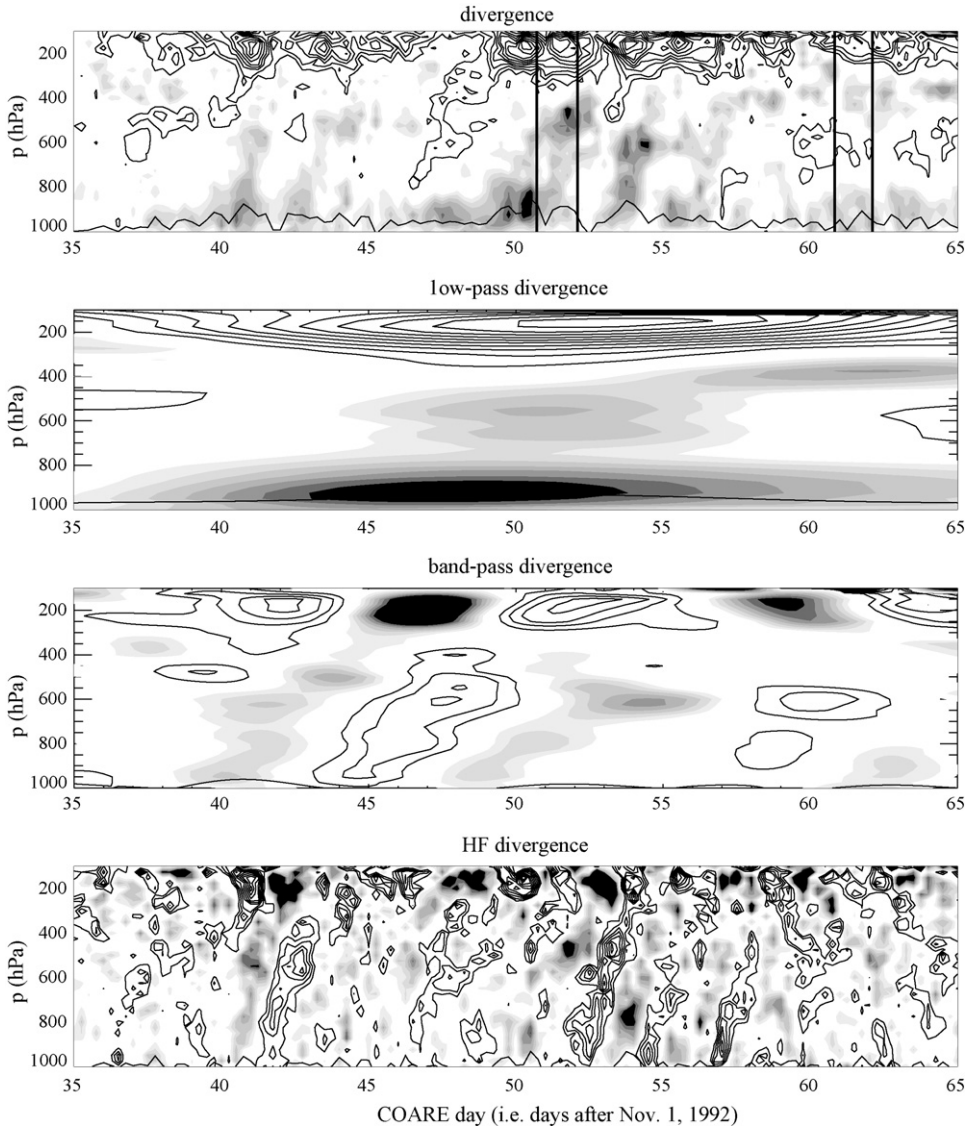

Fig. 8. Time–height OSA divergence data, raw (top) and temporally filtered (lower panels). Low-pass (LP, periods <20 days), band-pass (BP, periods 6–20 days), and high frequency (total − LP − BP) components are shown. Positive values are in open contours ($2 \times 10^{-6}\,s^{-1}$ linear interval in top, $1 \times 10^{-6}\,s^{-1}$ in lower panels). Negative values are shaded, with half the contour interval of positive values (open contours). Vertical bars indicate approximate times of satellite images in Fig. 9.

6. Null hypotheses for multiscale similarity

One null hypothesis for the self-similar tilted structure seen at different time scales in Fig. 8 is that the MCS life cycle is being aliased onto longer time scales through simple superposition. To test this hypothesis, we construct a synthetic divergence dataset using the OSA

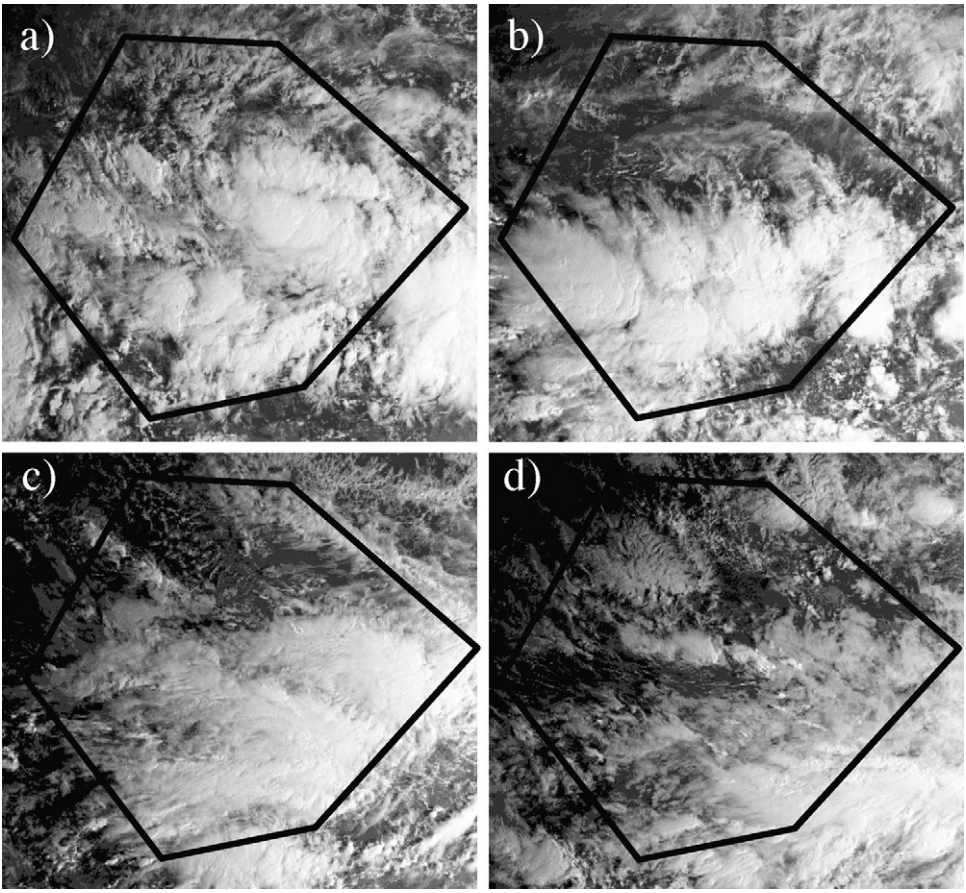

Fig. 9. Early morning visible satellite imagery in the OSA region (10S–10N, centered on ∼155E) for times highlighted in Fig. 8. (a) 20 UTC, 21 December 1992; (b) 20 UTC, 22 December 1992; (c) 20 UTC, 31 December 1992; (d) 20 UTC, 1 January 1993.

rainfall time series and composite MCS life cycle (Fig. 4a) as inputs. For each rainrate peak in the time series, a copy of this 24-h composite MCS regression structure is added to a synthetic divergence time–height section, with its amplitude scaled according to the peak rainrate for the event. In other words, the VAD-derived composite MCS evolution is treated as a fixed-structure 24-h "building block" for longer period variations indicated by the OSA rainrate time series.

This Building Block hypothesis completely fails to account for tilt at longer periods (Fig. 10a). Low-pass filtered time variations (not shown) consist merely of modulations in time of the 24 h-mean divergence profile of the building block. This failure is not too surprising, either mathematically or physically, since it is well known that not all tropical rainfall events consist of classic MCS structures with identical proportions of convective and stratiform rain.

One prominent way in which MCS events vary is in having different amounts of stratiform precipitation (and the associated divergence structure) following convective rainfall. Such variation can be found on many scales, e.g. between dry and wet epochs in these EPIC data

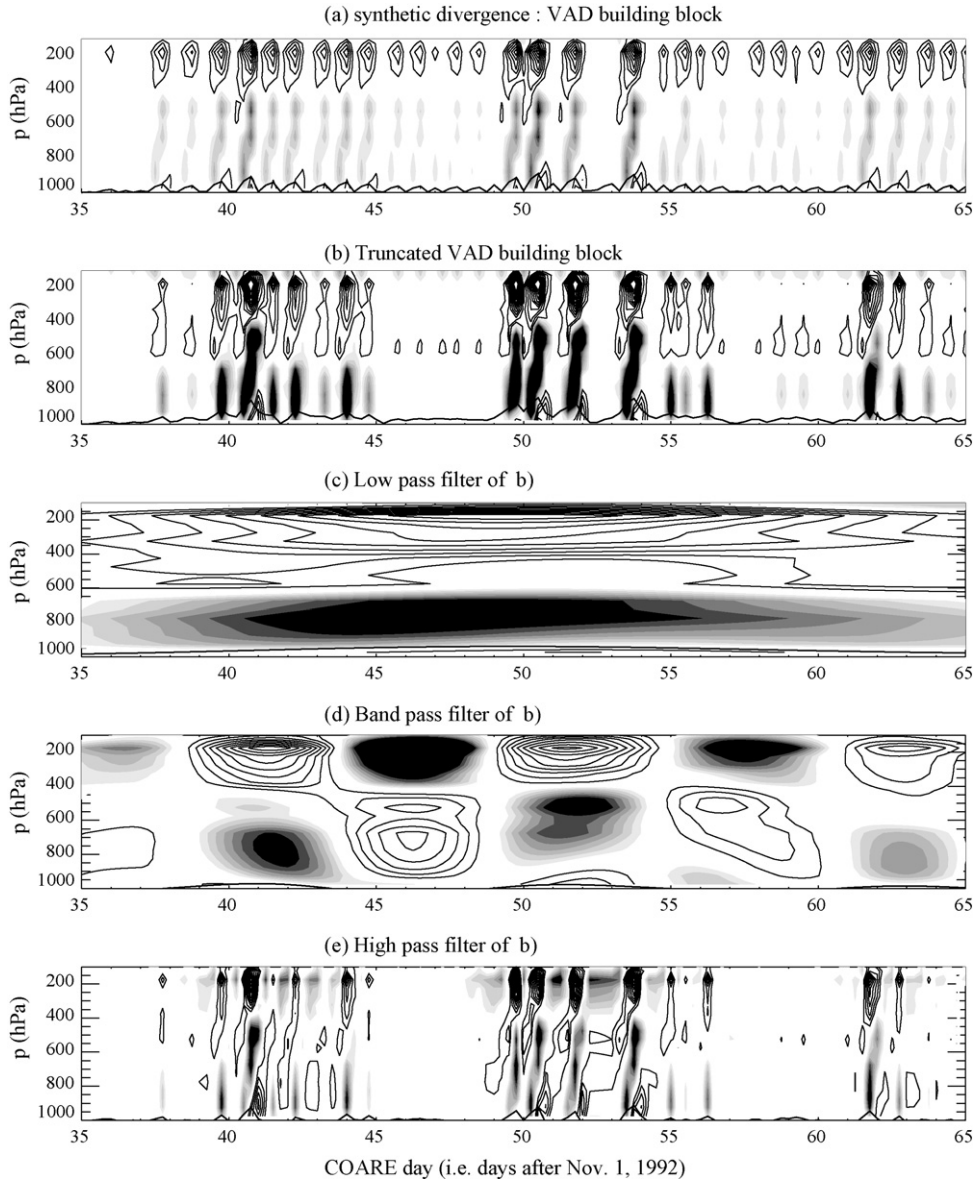

Fig. 10. As in Fig. 8, but for synthetic divergences, constructed by assigning to every peak in the OSA rainrate time series a characteristic structure derived from Fig. 4a. (a) The Building Block hypothesis, with Fig. 4a simply rescaled in magnitude according to time-dependent rainrate. (b) The truncated Building Block hypothesis, with rainrate used to terminate the MCS life cycle of Fig. 4a before its full 25-h completion. (c–e) Filtered versions of (b) as in Fig. 8.

(Petersen et al., 2003); or between eastern versus western Pacific, with global consequences (Schumacher et al., 2004). This common form of variation suggests an extension, the Truncated Building Block hypothesis, in which the composite MCS life cycle does not manage to proceed to completion during smaller rain events. Fig. 10b illustrates a synthetic data exercise based on

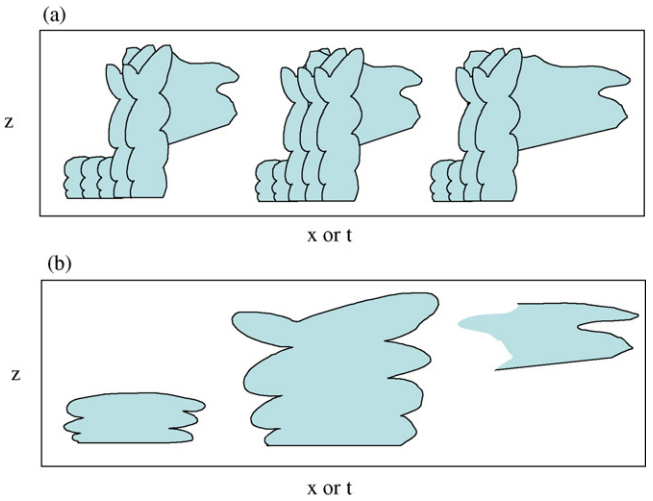

Fig. 11. Schematic of the "Stretched Building Block" hypothesis, depicting MCSs as three cloud types (shallow convective in left, deep convective in middle, and stratiform in right), within a large-scale wave structure whose environmental zones favor the cloud types differentially. When the mean is removed and smoothing broadens features, the resulting large-scale pattern resembles the MCS life cycle. (a) Unfiltered view; (b) low-pass filtered.

this notion, in which OSA rainrate peaks are again used to superpose composite VAD divergence time–height sections. This time, the later part of those 24-h sections is cut off at a time related monotonically to the magnitude of the large-scale rainrate peak. Many monotonic functions were tried, and Fig. 10 shows the best low-frequency tilt achieved in these experiments. The low-pass panel (Fig. 10c) and the band-pass panel (Fig. 10d) clearly lack the robust tilts seen in Fig. 8.

Instead, it appears that a satisfactory construction of multiscale tilted structure must involve something like summing the lower three panels of Fig. 8. In this view, which might be called the Stretched Building Block hypothesis, the low-frequency transition from low-level convergence to middle-level convergence – over days not hours – is *analogous to*, not merely an aliasing of, the transition from the early to late stages of an MCS. Such a view appears to require that the shallow cumulus, deep cumulonimbus, and precipitating stratiform anvil stages of a wave consist of *populations* of frequently refreshed clouds within large-scale 'zones' that favor them.

The Stretched Building Block conceptual model is summarized in Fig. 11. Here MCSs consist of three cloud types – shallow, deep, and anvil – but the relative abundance of these cloud types varies on a larger scale (top panel). In a filtered view (bottom panel), the larger scale wave evolution looks like a stretched version the MCS life cycle. But this view raises as many questions as it answers. In particular, how does the large-scale environment determine the amounts of the three cloud types? At least the efforts above may allow us to usefully rephrase the question: *how are the timing and durations of the stages of the MCS life cycle affected by the larger scale environment?* Fortunately, we may be able to use similarity (and differences) across scales to some advantage in addressing this question. The remainder of the paper attempts to deduce something about environmental modulation of cloud populations using data from an idealized cloud model simulation and from the noisier but real-world COARE IFA data. For brevity, our focus is on the leading-edge structure (shallow to deep convection transition), and on thermodynamic effects (buoyancy). The possibility of dynamical governors on cloud populations (e.g. wind shear) is acknowledged, but is more complex and will only be addressed briefly in our concluding discussion.

7. Waves and convection in a cloud model

Mesoscale convective systems have been hard to simulate in their totality, because the inner processes of updrafts, cloudiness, rainfall, and downdrafts require high resolution, while the outer process of gravity wave-mediated compensating subsidence spans thousands of kilometers. Such a range of scales has been computationally affordable in two-dimensional simulations for several years (Grabowski, 1998), and is now becoming feasible in 3D (Shutts, 2006; Tomita et al., 2005). In one recent 2D cloud-resolving radiative convective equilibrium simulation (Tulich et al., in press), spontaneously emerging large-scale (∼2500 km) propagating wave envelopes of moist convection activity have been diagnosed in detail. The key waves which appear to govern the large-scale propagation correspond to vertical wavenumbers 1–2 within the troposphere, interacting with three complete, mutually exclusive classes of objectively categorized cloudy columns: shallow convection (sometimes overlain by high cloud); deep convection; and stratiform anvils.

The model's regressed divergence structure (Fig. 12a) is generally similar to observations (Fig. 4a), although the convergence in advance of rainfall is much more tightly confined near the surface. The time scale of correlation decay at this 32 km spatial scale is ∼3 h, somewhat shorter than the ∼6 h in the 100 km scale observational picture in Fig. 4. Regression composites of the three types

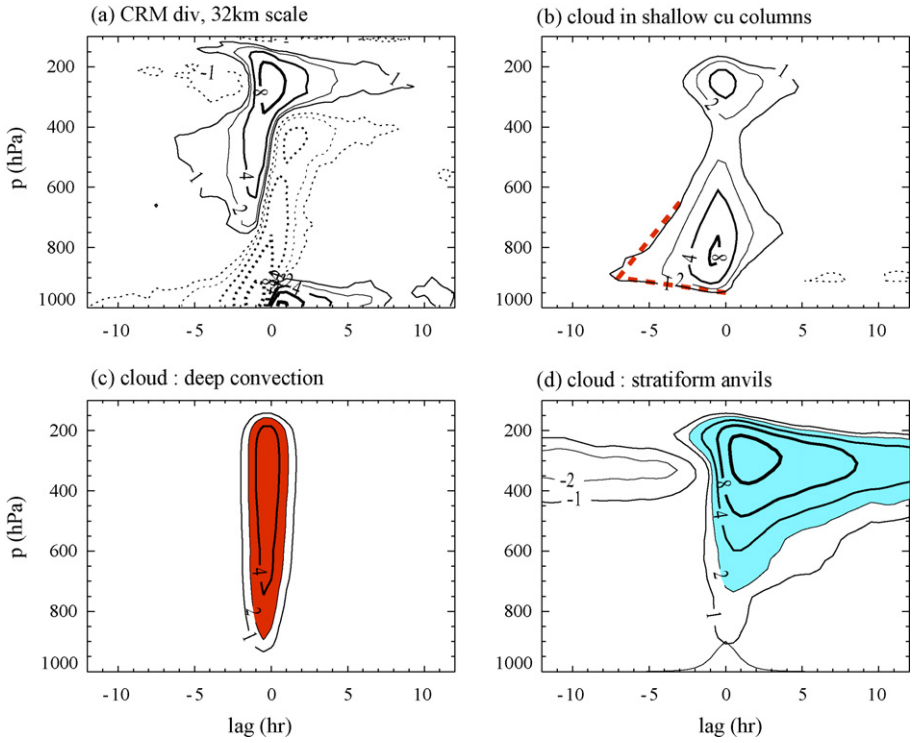

Fig. 12. Cloud model data at 32 km scale regressed against surface rainrate. (a) Divergence, (compare Fig. 4a), (b) shallow cumulus cloud cover, (c) deep convective cloud cover, and (d) stratiform anvil cloud cover. See Tulich et al. (in press) for details of cloud type definitions. Cloudiness contour unit 0.2% per mm/h. The positive part of the rainrate autocorrelation curve is plotted between 1000 and 900 h Pa at the base of panel (d). Shaded areas are annotations for Fig. 13.

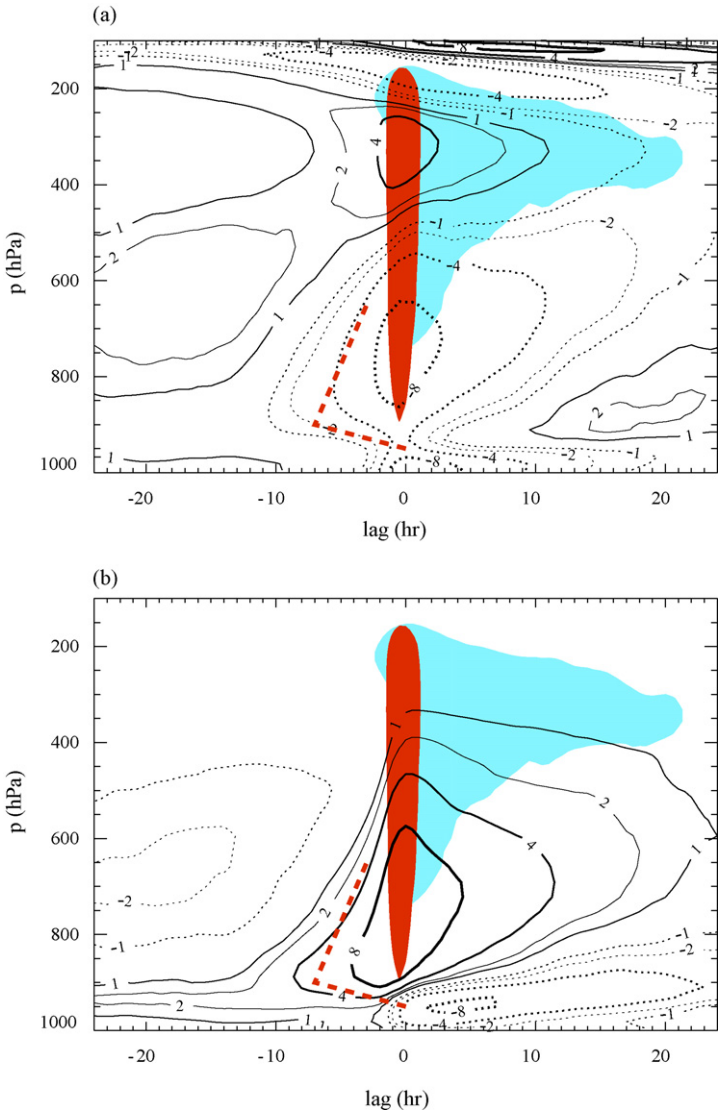

Fig. 13. Cloud model regressions of temperature T and specific humidity q, with the three cloud type regression annotations from Fig. 12 for reference. (a) CRM T: 0.03 K per mm/h; (b) CRM q: 0.03 g/kg per mm/h.

of cloudiness (shallow, deep, stratiform) are shown in panels b–d, with few surprises. Annotations in these panels (shadings and dashed angle curve) are overlain on regressed temperature (T) and specific humidity (q) structure in Fig. 13.

The T and q structures are quite smooth and coherent, both in and beyond the contours indicating cloud amounts. Cooling in the lower troposphere destabilizes the low-level lapse rate in advance of rainfall, while humidity anomalies also grow in strength and depth. Shallow convective clouds grow into this cool moist layer, where they experience enhanced buoyancy. When they pass the middle troposphere around lag −2 h, deep convection ensues, followed by stratiform anvil cloud.

While there are quantitative amplifications near the time of peak rainfall, T and q are much less localized than are clouds and the associated latent heating implied by the divergence in Fig. 12a or rainfall autocorrelation curve in Fig. 12d. We interpret this as indicating that the pattern of T should be interpreted as the density field of the large-scale wave, and not in terms of local heating or cooling rates (with the exception of the thin, rapidly developing layer of cold outflow at the surface).

Consider the increase of T with time in the 600–900 h Pa layer after peak rainfall. In this region, evaporating clouds and rain are known to comprise a diabatic cooling. No radiation is active, so cloud-base radiant warming cannot offset this. Yet T increases, indicating that the subsidence rate exceeds that required to offset diabatic cooling. This dominance of dynamical over diabatic tendency terms is also observed in nature, in the form of post-stratiform 'onion soundings' (Zipser, 1969, 1977) with their characteristic subsidence inversion structure in T and q. The thermally indirect nature of this descent led Miller and Betts (1977) to postulate that air is "forced or 'sucked' down," perhaps by the slumping of the cold pool at the surface. By similar reasoning, decreasing T in the anvil after rainfall reflects an ascent rate greater than that required to offset diabatic heating. This dynamical ascent must have important impacts on anvil longevity, even though the anvil may owe its *existence* to convective outflow.

8. Observations: temperature versus moisture effects on convection

The gross description of T and q regressions from unfiltered COARE IFA observations (Fig. 14) corresponds reasonably well to the model fields of Fig. 13: broadly, features slope upward with time. A wedge-shaped q structure rises upward in advance of precipitation, presumably as the cumulus cloud field deepens. After rain, this wedge is undercut by low-level drying. Meanwhile, T cools with time below about 400 h Pa before peak rainfall, while the upper troposphere warms slightly leading up to lag 0, then cools after rain. Cold air at the surface signifies rain evaporation.

In the days before peak rain, T and q anomalies seem to jump up discretely, suggesting cloud populations with tops near ∼750, 600, and <500 h Pa, as suggested by the heavy dashed annotation. This complex structure may reflect a more diverse set of cumulus cloud types (humilis, mediocris, congestus) than the model is able to resolve well. Layering in the T field also indicates a roughly 100–200 h Pa decorrelation scale, with layers of apparently independent variability centered near 900, 750, 600, 400, and 250 h Pa. A stable layer near the top of the moist layer appears to jump discretely along the same stair-step annotation.

The basic tilted shape of features seen here is common to other statistical studies of convection-associated sounding variations, from MCS case studies (Gamache and Houze, 1985), to statistical studies of soundings near convective events (Sherwood and Wahrlich, 1999), to 2-day waves (Haertel and Johnson, 1998; Takayabu et al., 1996), to Kelvin waves (Straub and Kiladis, 2003; Straub et al., 2006), to the Madden–Julian Oscillation (Kiladis et al., 2005). Regressions of T and q from the EPIC and JASMINE datasets used here also depict similar evolution, with complex lower-troposphere layering more like Fig. 14 than like Fig. 13 (not shown). Observations are often noisy and the signal is delicate, so these observed patterns have been difficult to interpret individually.

Two main time scales are evident in Fig. 14. There is a rapid decay of all variables within a ∼2-day window about the rain peak, then a slower decay out to edges of the full 10-day interval shown. The inner scale corresponds to MCSs and 2-day waves, while the longer time scale is substructure of the intraseasonal oscillation (recall Figs. 7 and 1e). It is notable that the lower-troposphere T anomalies decay more quickly with lag than do q anomalies, such that the *ratio* of rain-regressed

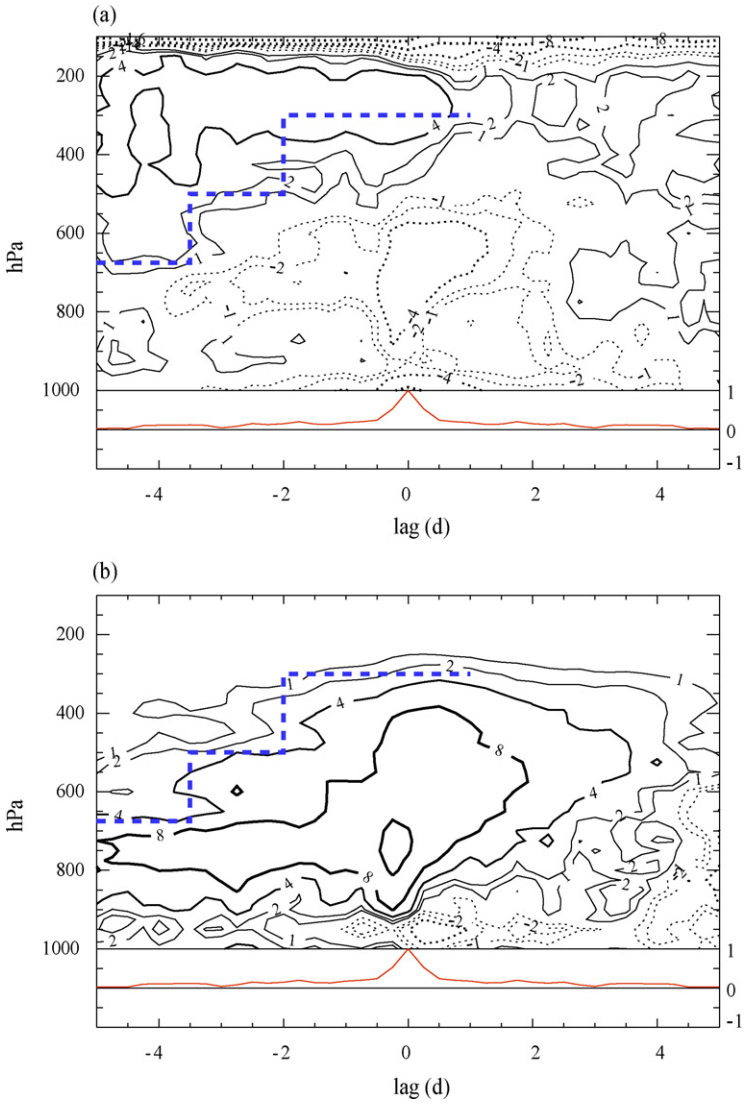

Fig. 14. COARE IFA lag regressions of T and q vs. moisture budget-derived rainrate. Autocorrelation curves (scale at right) are shown at the base of each panel. (a) IFA T: 0.060 K per mm/h; (b) IFA q: 0.060 g/kg per mm/h.

q to T anomalies appears to be smaller for fast (wavelike) variability, and larger for intraseasonal variations. In the case of Fig. 13, the cloud model's convection was clearly organized by gravity waves, which must propagate via the density (T) field, and are thought to orchestrate convection also through the T field. There the ratio of the magnitudes of lower-troposphere moistening (q) and cooling (T) anomalies is less than 2:1 (in g/kg:K units, respectively). In contrast, at lags < -2 days, Fig. 14 depicts q:T anomaly ratios exceeding 4:1.

This substantial difference of q:T ratio between convectively coupled waves and intraseasonal variability appears to be supported by other data. Our own analyses (not shown) indicate ratios near or less than 2:1 for the relatively fast variations in EPIC, in the easterly waves of the classic

GATE Atlantic experiment of 1974, and in the IFA data of Fig. 14 when they are high-pass filtered. In the published literature, results of Takayabu et al. (1996) and Straub and Kiladis (2003), and Fig. 9 of Straub et al. (2006) indicate similarly small ratios for 2-day waves and Kelvin waves, in contrast to q:T ratios well over 3 in Madden–Julian filtered regressions (Kiladis et al., 2005).

There are at least three physical metrics for interpreting this q:T ratio. One is via the virtual temperature effect (light molecular weight of water): in this measure, the q variations are simply unimportant. A second, more pertinent metric is moist static energy (accounting for latent heat), which makes q variations much more important. The latent heat in 1 g/kg of q is about 2.5 times the enthalpy in a 1 K T anomaly, so the density of an entraining saturated cumulus updraft is much more affected by an anomaly of 1 g/kg in q than by 1 K in T (Peters and Bretherton, in press). A third metric involves background vertical gradients of moisture and temperature. A vertical displacement acting on the time-mean COARE IFA sounding would induce anomalies with a q/T ratio of about 1 at 900 h Pa, 0.5 at 700 h Pa, and 0.25 at 500 h Pa. The observed q anomalies are several times larger than this, indicating that convective feedbacks act to strongly amplify the moisture variability relative to this adiabatic displacement value.

At least three processes could explain the relative largeness of q anomalies: (1) destabilization by wave cooling in the lower free troposphere might unleash a large eddy vertical q flux by cumulus clouds, many times greater than the vertical q flux by wave ascent itself. If this cumulus flux ventilates the boundary layer enough to compel extra surface flux of q, this flux could ultimately supply the growing and deepening q anomaly. (2) Shallow cumulus clouds induced by wave ascent might precipitate so much that net latent heating mostly balances wave-induced cooling. Ascent driven by a unit of latent heating will actually supply more than 1 unit of moisture convergence in a potentially unstable environment, where moist static energy decreases with height (as is the case below about 650 h Pa in the IFA mean sounding). As a result, q anomalies can actually be increased by the moisture sink of precipitation, if the circulation is shallow (Wu, 2003). (3) Surface flux induced by wind speed enhancements may be the driver of variability, so that free tropospheric T and q may both be consequences rather than causes of the life cycle of convection variations (Raymond et al., 2006). Cloud model sensitivity tests, adjusting shallow cumulus rain microphysics or surface flux formulations, might shed light on the relative importance of these mechanisms (if the entire character of variability does not change too much).

Here we conclude with a simple buoyancy diagnosis of the relative importance of q and T as causal agents in convection variations. Fig. 15 shows regressions of entraining plume buoyancy and its components, using as inputs the mean sounding at each time in the COARE IFA time–height series. The computed time–height sections of plume density temperature T_ρ (or buoyancy, T_ρ minus the environmental T_v profile) were regressed just like any other dataset. Using the full plume buoyancy, but only where it is positive (this helps with figure clarity at upper levels) yields Fig. 15a. The plume calculation appears to have some explanatory skill: it shows extra buoyancy in association with rain, and in advance of rain at low levels where enhanced shallow convection occurs. Strong entrainment was used, corresponding to a 500 m radius plume in the pressure coordinate scheme of Kain and Fritsch (Kain, 2004). The ‘correct’ value of this parameter for representing the rate-limiting stages of convective development is unknown. Sensitivity of the result is fairly weak, though, so long as the inverse of the entrainment rate does not become very large with respect to the depth of q anomalies (not shown).

The sources of this result are broken down in the other panels of Fig. 15. Pure lifted-PBL T_ρ is greater for pre-rain than post-rain conditions, because of greater q near the surface (Fig. 14b). But outflow air near the surface during rain has especially low T_ρ when lifted, causing

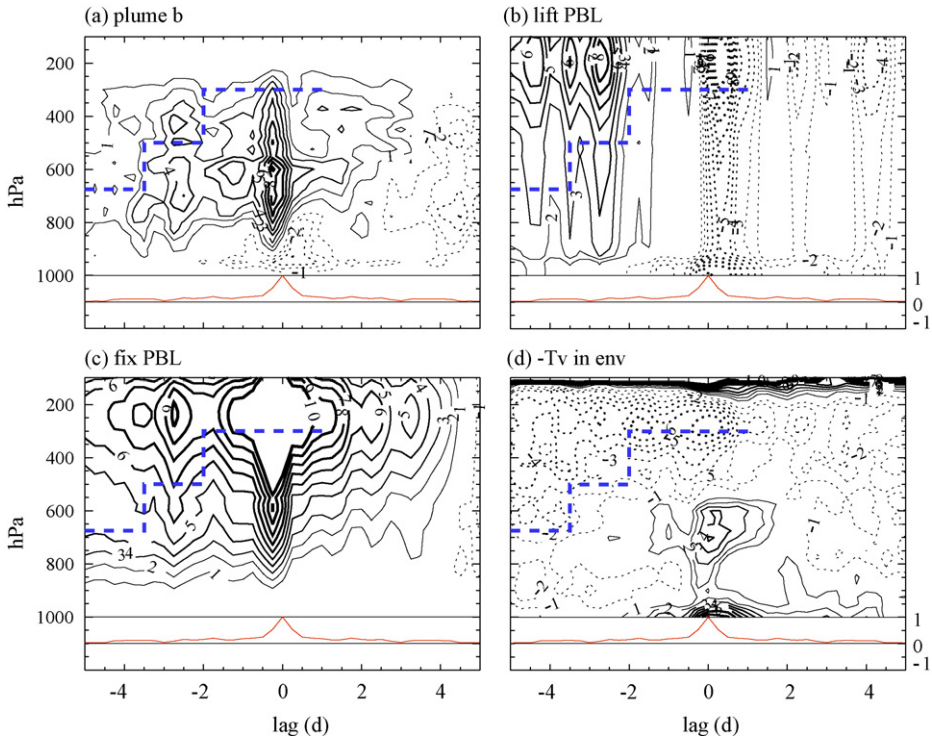

Fig. 15. Lag-height regressions vs. COARE IFA rainrate of quantities related to an entraining plume buoyancy (expressed in density-temperature units), computed from COARE IFA thermodynamic profile data. Linear contours are used in this figure, ranging from −10 to 10 in units of 6 cK per mm/h. (a) Plume buoyancy with negative values truncated at 0. The plume has a Kain–Fritsch entrainment scheme in pressure, with radius 500 m. (b) Density temperature of lifted parcels of air obtained by mixing the 1000, 975, and 950 h Pa layer at each time. (c) Density temperature of entraining plumes, with the cloud-base plume thermodynamics set by time-mean T and q mixed over 1000, 975, and 950 h Pa. (d) The negative of COARE IFA virtual temperature.

an oft-rediscovered negative correlation between rain and naively computed simultaneous parcel instability. The effect of conditions above the boundary layer is isolated in panel c, for which time-mean PBL conditions (lowest 50 h Pa) were fed into the base of the entraining plume at each time. The q field above the surface dominates this result, and its effect is enough to overcome the PBL effect near lag 0, to yield the positive buoyancy anomalies seen there in panel a. Panel d shows the environmental T_v contribution to buoyancy. For the high-frequency part of the pattern, near lag 0, T explains almost half the enhanced buoyancy at about the 700 h Pa level. Meanwhile the environmental warmth aloft decreases upper-level buoyancy, but not enough to stop deep convection. The resulting heating-temperature correlation implies an important energy transfer from convection to large-scale flow.

In the annotated upward steps of convection top height at negative lags, the weakening of capping temperature anomalies above each step (panel d) is comparable to other effects, and so may be hypothesized to play a role in the intraseasonal evolution. On the other hand, these changes are tiny in absolute terms (fractions of a degree), and are in the sense of cumulus impacts (cooling and moistening at cloud top where liquid water is detrained). Indeed, the whole notion that convective changes are governed through buoyancy effects caused by slight environmental T

and q changes may be questioned: these changes could be consequences of convection variations governed in some other way, perhaps through the wind field, for example.

To more convincingly tease apart the sensitivities of convection and cloud "zones" to large-scale wave mechanisms will require experimentation with cloud-resolving models. A first attempt at mapping deep convective cloud sensitivities is described in Mapes et al. (2004), where q and T impacts on rainfall were found to be about equal for anomalies with relative magnitudes corresponding to adiabatic vertical displacement. Additional work is underway, and appears to support that result (not shown). Since the observed q anomalies are a few times larger than adiabatic, the first-order importance of q to deep updraft buoyancy seen in Fig. 15 and deduced by Peters and Bretherton (in press) may be correct. However, since those large q anomalies are deduced to be the product of shallow convective feedbacks, overall wave modulation of deep convection may need to be viewed as a more complex process, involving a shallow convection q 'amplifier' of signals which may still originate in the T field.

9. Summary and discussion

The upward growth of convection, and its transition to precipitating stratiform anvil cloudiness, has been seen to shape the evolution of tropical weather at various scales. The most familiar scale is the individual convective cloud or MPF (Leary and Houze, 1979), as seen in high-resolution radar or rain gauge data. This lower limit to the timescale spectrum is apparently set by processes of cumulus dynamics, precipitation microphysics, and multicellular aggregates of these, as precipitation-generated cold pools trigger new convective cells. A quasi-universal mesoscale structure is seen (Figs. 4–6) from multiple deployments across the tropics (Mapes and Lin, 2005).

Data averaged over increasingly large space scales tend to have relatively more variability at low frequency (or really, less variability at high frequency). As a result, the dominant or 'characteristic' decorrelation time scale in a dataset varies with resolution (Fig. 3). Nonetheless, multiple time scales are superposed in even the largest scale datasets used here, and filtering can tease these time scales apart (Fig. 7).

A satisfying explanation of the multiscale similarity appears to require a Stretched Building Block conceptual model (Fig. 11), in which individual cloud systems (thunderstorms or MPFs) in different phases of a large-scale wave have different *durations* of shallow convective, deep convective, and stratiform anvil stages in their life cycles. This raises the question of how a cloud system 'knows' what phase of a large-scale wave it is in. Here we turned attention mainly to thermodynamic variables (T and q), especially at low levels in the early stages of the life cycle.

Wavy convection variations, i.e. those which satisfy dispersion relations for large-scale density waves, offer an important baseline. Here we can confidently infer that density (temperature) effects must be important in orchestrating convection. Yet even in the case of an especially pure model simulation of wave-modulated convection (Fig. 13), important moisture and shallow convection feedbacks are evident in the large magnitude of q anomalies. On intraseasonal time scales, moisture effects are even more important, which may somehow underlie the well defined distinction between Kelvin waves and the Madden–Julian Oscillation (Wheeler and Kiladis, 1999).

The duration of stratiform anvil cloud zones is governed by very different physical processes than shallow cumulus clouds. (One concern about statistical studies which use filtering is that an artificial antisymmetry may be introduced between the shallow convective and stratiform anvil zones.) How long can stratiform anvil cloudiness and precipitation persist after their deep convective source has disappeared? The observation of a long-lasting elevated convergence layer in the last several days of Fig. 8a (implying upper-level ascent and clouds, cf. Fig. 9c and d) is

notable. We have seen that there can be wave-dynamical demands for upper-tropospheric density (cooling in excess of diabatic heating, Fig. 13), which can be important for cloud formation and persistence (Boehm and Verlinde, 2000), especially in light of neutral moist stability in the upper troposphere (Johnson and Kriete, 1982). A recent Lagrangian study of tropical upper-level clouds (Luo and Rossow, 2004) shows that cirrus clouds can be tracked for several days after the time of last convection (although Fig. 9 is a useful sobriety check on the possible inaccuracies of such an exercise). Radiative heating of post-convective anvil clouds extends their lifetimes (Webster and Stephens, 1980), while wind shear systematically expands their coverage (Lin and Mapes, 2004; Saxen and Rutledge, 2000). In short, no strongly binding upper limit to the longevity of anvil clouds, or to the ratio of anvil cloudiness to deep convective cloudiness, can be easily invoked.

Besides defining a lower limit on time scale, convective cloud processes may also constrain phase relations in the moist tropical wave spectrum. We speculate that there is a natural selection in the atmosphere for wave packets whose phase structure produces a local, Eulerian sequence of cloud zone-supporting anomalies that aligns with the convective cloud system life cycle. Oppositely phased wave groups may exist, but fail to engage or 'pattern' the convection field (Lindzen, 2003), with negative consequences for at least their observability, and probably also for their coherence. These notions may be usefully testable in simple discretized tropical wave models, with two vertical wavenumber dynamics and three cloud types (Khouider and Majda, 2006; Mapes, 2000), perhaps calibrated with CRM results (Tulich et al., in press).

On the flip side, scale similarity raises questions at the mesoscale. How well do we understand the fundamental reasons for the life cycle of MCSs? Despite decades of recognition and study, many mysteries remain (Houze, 2004), and the sense of familiarity arising from masses of observational data can get in the way of recognizing and asking basic questions. With the rise of numerical modeling, gravity wave effects in and around MCSs have become a much more feasible object of study. From their 'inner' roles in MCS inflows and outflows (Pandya and Durran, 1996) and even cellularity in the convective region (Yang and Houze, 1995), to their 'outer' roles in convective initiation and propagation (Lac et al., 2002), gravity waves have taken their place alongside cold pools as a major shaping force in mesoscale convection. It is not clear what truly new thing can be learned about MCSs from smooth, simple composite results like Fig. 4, but similarity across scales at least suggests that asking and answering the relevant questions may have a broader significance to a wider community.

Acknowledgements

This material is based upon work supported by the National Science Foundation under grants ATM-0097116, 0407559, 0336790, and 0112715. Discussions with George Kiladis helped inspire and enrich this work. Paul Ciesielski kindly provided the latest versions of the COARE IFA and OSA datasets. His comments and those of Bob Houze, Richard Johnson, Andy Majda, and anonymous reviewers greatly improved the manuscript.

References

Biello, J.A., Majda, A.J., 2005. A new multiscale model of the Madden–Julian Oscillation. J. Atmos. Sci. 62, 1694–1722.

Biello, J.A., Majda, A.J., 1998. Modulating synoptic scale convective activity and boundary layer dissipation in the IPESD models of the Madden–Julian Oscillation. Dyn. Atm. Oceans 42, 152–215.

Boehm, M.T., Verlinde, J., 2000. Stratospheric influence on upper tropospheric tropical cirrus. Geophys. Res. Lett. 27, 3209–3212.

Ciesielski, P.E., Johnson, R.H., Haertel, P.T., Wang, J., 2003. Corrected TOGA COARE sounding humidity data: impact on diagnosed properties of convection and climate over the Warm Pool. J. Clim. 16, 2370–2384.

Gamache, J.F., Houze, R.A., 1985. Further analysis of the composite wind and thermodynamic structure of the 12 September GATE squall line. Mon. Wea. Rev. 113, 1241–1259.

Grabowski, W.W., 1998. Toward cloud resolving modeling of large-scale tropical circulations: a simple cloud microphysics parameterization. J. Atmos. Sci. 55, 3283–3298.

Grabowski, W.W., Moncrieff, M.W., 2001. Large-scale organization of tropical convection in two-dimensional explicit numerical simulations. Q. J. R. Met. Soc. 127, 445–468.

Guichard, F., Parsons, D., Miller, E., 2000. Thermodynamic and radiative impact of the correction of sounding humidity bias in the tropics. J. Clim. 13, 3611–3624.

Haertel, P., Kiladis, G.N., 2004. Dynamics of 2-day equatorial waves. J. Atmos. Sci. 61, 2707–2721.

Houze, R.A., Jr., 1982. Cloud clusters and large-scale vertical motion in the tropics. J. Meteor. Soc. Japan 60, 396–410.

Haertel, P.T., Johnson, R., 1998. Two-day disturbances in the equatorial western Pacific. Q. J. R. Meteor. Soc. 124, 615–636.

Houze, R.A., 1993. Cloud Dynamics. Academic Press, San Diego, CA.

Houze, R.A., 1997. Stratiform precipitation in regions of convection: a meteorological paradox? Bull. Am. Meteorol. Soc. 78, 2179–2196.

Houze, R.A., 2004. Mesoscale convective systems. Rev. Geophys. 42, doi:10.1029/2004RG000150.

Houze, R.A., Chen, S.S., Kingsmill, D.E., Serra, Y., Yuter, S.E., 2000. Convection over the Pacific warm pool in relation to the atmospheric KelvinRossby wave. J. Atmos. Sci. 57, 3058–3089.

Johnson, R.H., Kriete, D.C., 1982. Thermodynamic and circulation characteristics of winter monsoon tropical mesoscale convection. Mon. Wea. Rev. 110, 1898–1911.

Johnson, R.H., Rickenbach, T., Rutledge, S.A., Ciesielski, P., Schubert, W., 1999. Trimodal characteristics of tropical convection. J. Clim. 12, 2397–2418.

Johnson, R.H., Ciesielski, P.E., 2000. Rainfall and radiative heating rates from TOGA COARE atmospheric budgets. J. Atmos. Sci. 57, 1497–1514.

Kain, J.S., 2004. The Kain-Fritsch convective parameterization: an update. J. Appl. Met. 43, 170–181.

Khouider, B., Majda, A.J., 2006. Model multicloud parameterizations for convectively coupled waves: detailed nonlinear wave evolution. Dyn. Atmos. Oceans 42, 59–80.

Kiladis, G.N., Weickmann, K., 1992. Circulation anomalies associated with tropical convection during northern winter. Mon. Wea. Rev. 120, 1900–1923.

Kiladis, G.N., Straub, K.H., Haertel, P.T., 2005. Zonal and vertical structure of the Madden–Julian Oscillation. J. Atmos. Sci. 62, 2790–2809.

Lac, C., Lafore, J.-P., Redelsperger, J.-L., 2002. Role of gravity waves in triggering deep convection during TOGA COARE. J. Atmos. Sci. 59, 1293–1316.

Leary, C.A., Houze, R.A., 1979. The structure and evolution of convection in a tropical cloud cluster. J. Atmos. Sci. 36, 437–457.

Lilly, D.K., 1960. On the theory of disturbances in a conditionally unstable atmosphere. Mon. Wea. Rev. 88, 1–17.

Lin, J.L., Mapes, B., 2004. Wind shear effects on cloud-radiation feedback in the western Pacific warm pool. Geophys. Res. Lett. 31, doi:10.1029/2004GL020199.

Lin, J.L., et al, 2006. Tropical intraseasonal variability in 14 IPCC AR4 climate models. Part I: convective signals. J. Clim. 19, 2665–2690.

Lin, X., Johnson, R.H., 1996. Kinematic and thermodynamic characteristics of the flow over the western Pacific warm pool during TOGA COARE. J. Atmos. Sci. 53, 695–715.

Lindzen, R.S., 2003. The interaction of waves and convection in the Tropics. J. Atmos. Sci. 60, 3009–3020.

Luo, Z., Rossow, W.B., 2004. Characterizing tropical cirrus life cycle, evolution, and interaction with upper tropospheric water vapor using Lagrangian trajectory analysis of satellite observations. J. Clim. 17, 4541–4563.

Mapes, B.E., 2000. Convective inhibition, subgrid-scale triggering energy, and stratiform instability in a toy tropical wave model. J. Atmos. Sci. 57, 1515–1535.

Mapes, B.E., Houze, R.A., 1993. Cloud clusters and superclusters over the oceanic warm pool. Mon. Wea. Rev. 121, 1398–1415.

Mapes, B.E., Lin, J., 2005. Doppler radar observations of mesoscale wind divergence in regions of tropical convection. Mon. Wea. Rev. 133, 1808–1824.

Mapes, B.E., Wu, X., 2001. Convective eddy momentum tendencies in long cloud-resolving model simulations. J. Atmos. Sci. 58, 517–526.

Mapes, B.E., Cielski, P.E., Johnson, R.H., 2004. Sampling errors in rawinsonde-array budgets. J. Atmos. Sci. 60, 2697–2714.

May, P.T., Rajopadhyaya, D.K., 1999. Vertical velocity characteristics of deep convection over Darwin, Australia. Mon. Wea. Rev. 127, 1056–1071.

McAnelly, R.L., Cotton, W.R., 1992. Early growth of mesoscale convective complexes: a meso-beta-scale cycle of convective precipitation? Mon. Wea. Rev. 120, 1851–1877.

Meehl, G.A., Lukas, R., Kiladis, G., Weickmann, K., Matthews, A., Wheeler, M., 2001. A conceptual framework for time and space scale interactions in the climate system. Clim. Dyn. 15, 753–775.

Miller, M.J., Betts, A.K., 1977. Traveling convective storms over Venezuela. Mon. Wea. Rev. 105, 833–848.

Moncrieff, M.W., 1992. Organized convective systems: archetypal dynamical models, mass and momentum flux theory, and parameterization. Q. J. R. Meteorol. Soc. 118, 819–850.

Moncrieff, M.W., 2004. Analytic representation of the large-scale organization of tropical convection. J. Atmos. Sci. 61, 1521–1538.

Morita, J., Takayabu, Y.N., Shige, S., Kodama, Y., 2006. Analysis of rainfall characteristics of the Madden–Julian Oscillation using TRMM satellite data. Dyn. Atmos. Oceans 42, 107–126.

Pandya, R.E., Durran, D.R., 1996. The influence of convectively generated thermal forcing on the mesoscale circulation around squall lines. J. Atmos. Sci. 53, 2924–2951.

Peters, M.E., Bretherton, C.S. Structure of tropical variability from a vertical mode perspective. Theor. Comp. Fluid. Dyn., in press.

Petersen, W.A., Cifelli, R., Boccippio, D.J., Rutledge, S.A., Fairall, C., 2003. Convection and easterly wave structures observed in the eastern Pacific warm pool during EPIC-2001. J. Atmos. Sci. 60, 1754–1773.

Raymond, D.J., Bretherton, C.S., Molinari, J., 2006. Dynamics of the intertropical convergence zone of the east Pacific. J. Atmos. Sci. 63, 582–597.

Raymond, D.J., et al., 2004., EPIC2001 and the coupled ocean-atmosphere system of the tropical east Pacific. Bull. Am. Meteor. Soc. 85, 1341–1354.

Ricciardulli, L., Sardeshmukh, P.D., 2002. Local time- and space scales of organized tropical deep convection. J. Clim. 15, 2775–2790.

Saxen, T.R., Rutledge, S.A., 2000. Surface rainfall cold cloud fractional coverage relationship in TOGA COARE: a function of vertical wind shear. Mon. Wea. Rev. 128, 407–415.

Schumacher, C., Houze, R.A., Kraucunas, I., 2004. The tropical dynamical response to latent heating estimates derived from the TRMM precipitation radar. J. Atmos. Sci. 61, 1341–1358.

Sherwood, S.C., Wahrlich, R., 1999. Observed evolution of tropical deep convective events and their environment. Mon. Wea. Rev. 127, 1777–1795.

Shutts, G., 2006, Simulations of tropical convection on an equatorial beta-plane. Dyn. Atmos. Oceans 42, 30–58.

Straub, K.H., Kiladis, G.N., 2003. The observed structure of convectively coupled kelvin waves: comparison with simple models of coupled wave instability. J. Atmos. Sci. 60, 1655–1668.

Straub, K.H., Kiladis, G.N., Ciesielski, P.E., 2006. The role of equatorial waves in the onset of the South China Sea summer monsoon and the demise of El Niño during 1998. Dyn. Atmos. Oceans 42, 216–238.

Takayabu, Y.N., 1994. Large-scale cloud disturbances associated with equatorial waves. Part I: spectral features of the cloud disturbances. J. Meteor. Soc. Jpn. 72, 433–448.

Takayabu, Y.N., Lau, K.-M., Sui, C.-H., 1996. Observation of a quasi-2-day wave during TOGA COARE. Mon. Wea. Rev. 124, 1892–1913.

Tomita, H., Miura, H., Iga, S., Nasuno, T., Satoh, M., 2005. A global cloud-resolving simulation: preliminary results from an aqua planet experiment. Geophys. Res. Lett. 32, L08805, doi:10.1029/2005GL022459.

Tulich, S., Randall, D.A., Mapes, B.E. Vertical-mode and cloud decomposition of large-scale convectively coupled gravity waves in a two-dimensional cloud resolving model. J. Atmos. Sci., in press.

Webster, P., et al., 2002., The JASMINE pilot study. Bull. Am. Meteor. Soc. 83, 1603–1630.

Webster, P.J., Lukas, R., 1992. TOGA COARE: the coupled ocean–atmosphere response experiment. Bull. Am. Meteor. Soc. 73, 1377–1416.

Webster, P.J., Stephens, G.L., 1980. Tropical upper-tropospheric extended clouds: inferences from winter MONEX. J. Atmos. Sci. 37, 1521–1541.

Wheeler, M., Kiladis, G.N., 1999. Convectively coupled equatorial waves: analysis of clouds and temperature in the wavenumber-frequency domain. J. Atmos. Sci. 56, 374–399.

Wilcox, E.M., Ramanathan, V., 2001. Scale dependence of the thermodynamic forcing of tropical monsoon clouds: results from TRMM observations. J. Clim. 14, 1511–1524.

Wu, Z., 2003. A shallow CISK, deep equilibrium mechanism for the interaction between large-scale convection and large-scale circulations in the tropics. J. Atmos. Sci. 60, 377–392.

Yang, M.-J., Houze, R.A., 1995. Multicell squall-line structure as a manifestation of vertically trapped gravity waves. Mon. Wea. Rev. 123, 641–661.

Zipser, E.J., 1969. The role of organized unsaturated convective downdrafts in the structure and rapid decay of an equatorial disturbance. J. Appl. Meteor. 8, 799–814.

Zipser, E.J., 1977. Mesoscale and convective-scale downdrafts as distinct components of squall-line structure. Mon. Wea. Rev. 105, 1568–1589.

Zipser, E.J., Meitin, R.J., LeMone, M.A., 1981. Mesoscale motion fields in association with a GATE convection band. J. Atmos. Sci. 38, 1725–1750.

Zuidema, P., Mapes, B., Lin, J., Fairall, C., Wick, G., 2006. The interaction of clouds and dry air in the eastern tropical Pacific. J. Clim. 19(18), 4531–4544.